Supplement of Upper tropospheric pollutants observed by MIPAS: geographic and seasonal variations

N. Glatthor[1], G. P. Stiller[1], T. von Clarmann[1,†], B. Funke[2], S. Kellmann[1], and A. Linden[1]

[1]Karlsruhe Institute of Technology, Institute of Meteorology and Climate Research, Karlsruhe, Germany
[2]Instituto de Astrofísica de Andalucía, CSIC, Granada, Spain
[†]deceased, 13 January 2024

Correspondence: N. Glatthor (norbert.glatthor@kit.edu)

1 MIPAS Tropopause heights

Exemplarily, the heights of the thermal tropopause derived from MIPAS temperature profiles obtained during the periods December 2009 to February 2010, March to May, June to August and September to November 2010 are displayed in Fig. S1. Especially during austral winter (Fig. S1c) a considerable number of unplausible high tropopause heights of up to 22 km was calculated for latitudes south of 60°S. Following the approach of Zängl and Hoinka (2001), tropopause heights above 90 hPa (∼14.7 km) generally were fixed to 14.7 km in this latitude band. Since quite a lot of unplausible high tropopause heights were also calculated for high northern latitudes during boreal winter (Fig. S1a) the same restriction was applied for latitudes north of 60°N.

2 Transport pathways

2.1 Northern hemispheric pollution during boreal spring

On 18 April 2007 a plume of strongly enhanced HCN was measured at 12 km altitude in a region extending from North-East Africa to South India (Fig. S2, top left). Eleven days later, on 29 April 2007, this enhancement had disappeared, but there was a large plume of high HCN above the northern subtropical Pacific (Fig. S2, top right). To investigate a connection between these two observations, 12-day HYSPLIT forward trajectories were started on 18 April, 0:00 UT, at 12 km altitude in the plume region above North-East Africa and the northern Indian Ocean (Figure S2, bottom). Here only the end sections of the trajectories covering the 29th of April are shown, colour coded by their altitude. They clearly indicate that the plume observed on April 29 above the western and central Pacific has been advected from North-East Africa. Moreover, the smaller HCN plume above northern Mexico/Texas can also be associated to the African source region.

Figure S3 (top left) shows a plume of enhanced HCN observed on 24 May 2007 at 8 km altitude above Western Europe. To identify potential source regions, HYSPLIT 12-day backward trajectories were started from this event (Fig. S3, top right). A considerable part of them originates on 12/13 May in the boundary layer abover Yucatan/Mexico and the Carribean Sea. Fire

counts of the Moderate Resolution Imaging Spectroradiometer (MODIS) (Justice et al., 2002) on the Aqua and Terra satellites, using the NASA Fire Information for Resource Management System (FIRMS) (see https://firms.modaps.eosdis.nasa.gov/, last access 22 February 2024) from 12–13 May 2007 (Fig. S3, bottom) show intensive biomass burning in Central America as well as in northern Venezuela. Thus, the HCN plume observed above Western Europe obviously was produced in these fire regions.

On 10 April 2008, a plume of enhanced HCN was observed at 8 km altitude at the West Coast of the U.S.A. (Figure S4, top left). A significant part of the HYSPLIT 12-day backward trajectories started from this event (Figure S4, top right) ends in the boundary layer above South-East-Asia, where FIRMS fire counts from 29 March 2008 show strong biomass burning (Fig. S4, bottom). This strongly hints to South-East-Asia as source region of the observed HCN plume.

2.2 Northern hemispheric pollution during boreal summer

As an example of northern hemispheric pollution during boreal summer, Figure S5 (top left) shows the global HCN distribution of 15 August 2010, measured at 8 km altitude. Here we focus on the origin of two plumes above North-Eastern Siberia (marked by red square). A considerable part of the HYSPLIT 13-day backward trajectories released from the area covering the plumes enters the boundary layer above Central Asia and passes the region eastward of Moscow on 3 August 2010 (Figure S5, top right). MODIS fire counts of this day indicate strong forest and peat fires in this region (Fig. S5, bottom), which obviously are the source of the plumes observed above North-Eastern Siberia.

Figure S6 (top left) shows boreal forest fires deteted by MODIS on 1 August 2010 in North-East Siberia. On this day a low pressure system approached the fire region from south-westward direction (see https://psl.noaa.gov/data/composites/day/), which in addition to the fire radiative power lead to an effective upward transport of the polluted air masses into the upper troposphere. To investigate the propagation of pollutants from this event, 11-day HYSPLIT forward trajectories were calculated, starting on 1 August, 0:00 UT, at 5 km above this region (top right). Here only the sections of the trajectories covering the August 11 are shown. The starting height of 5 km was chosen taking into account a plume injection height of 3 km and the uplift by the low pressure system. The injection height of 3 km was estimated using the MISR Enhanced Research and Lookup Interface (MISR/MERLIN) (see https://asdc.larc.nasa.gov/documents/misr/guide/MERLIN_User_Guide.pdf, last access 22 February 2024), which provides smoke plume heights measured by the Multi-Angle Imaging SpectroRadiometer (MISR) experiment on the Terra satellite.

On 11 August 2010, strongly enhanced HCN was detected in various regions of the northern hemisphere (bottom). By means of the trajectories, various plumes of enhanced HCN measured on 11 August can be associated to the source region in North-Eastern Siberia. In detail, this are the plumes above Kamtschatka and the source region itself, above Novaja Semlja and northern central Siberia, above Great Britain and Southern Scandinavia, Labrador and the Canadian Arctics.

2.3 Southern hemispheric pollution during austral winter and spring

Figure S7 shows 12-day HYSPLIT forward trajectories, started on 2 August 2010 at 3 km altitude above tropical South America, which illustrate transport of these air masses - potentially polluted by HCOOH from biogenic release - into the upper troposphere at southern hemispheric mid-latitudes.

Figure S8 shows 13-day HYSPLIT forward trajectories, started on 1 October 2010 at 12 km altitude above the biomass burning regions in Brazil (top left) and South Africa (top right) as well as on 1 October 2006 at 13 km altitude above Indonesia (bottom). The trajectories show that biomass burning in each of these regions can contribute to southern hemispheric pollution observed in southern hemispheric spring. During the displayed time period, South American pollution is mainly transported south-eastward towards the subtropical southern Atlantic, South Africa, the subtropical Indian Ocean and Australia, but partly westward to the tropical Pacific as well. From there some trajectories even enter the northern hemisphere and cross the Gulf of Mexico towards the Atlantic. The major part of South African pollution is also transported south-eastward to the tropical and subtropical Indian Ocean, Australia, the tropical and subtropical Pacific and the southern Atlantic. Another transport path extends westward above the tropical Atlantic to Brazil. Pollution from Indonesia is transported both in eastward and westward direction, and covers the whole southern tropical and subtropical Pacific and Indian Ocean as well as the subtropical southern Atlantic.

3 Correlation plots

As an example for the data sets underlying the plots in Figs. 9-13 of the main manuscript, Figure S9 shows correlation plots between the September (left) and October composites (right) of MIPAS C_2H_2 and HCN at 3 km below the tropopause for a bin between Mozambique (Southern Africa) and southern Madagascar (22.5°S-27.5°S, 30°E-45°E). The latter plot corresponds to the respective bin displayed in Fig. 10 of the main manuscript. The correlation is high in September ($r = 0.77$) and very high in October ($r = 0.91$). The ERs fitted for this data set are 0.48 and 0.30 for September and October, respectively, which is close to the mean ERs given for South Africa in Tab. 4 of the main manuscript. Correlation plots for September (left) and October (right) of the individual years 2002, 2007 and 2010 are displayed in the rows below. The correlation coefficients are mostly even somewhat higher than for the monthly composites. The ERs calculated for the different years show large differences, but a common feature with the composite plots is the strong decrease from September to October. Thus, in every single year as well as in the composites we see a clear indication of aging pollution.

In Figure S10 we show C_2H_2-HCN correlation plots for the September (left) and October composites (right) for the whole southern Africa (30°S-0°S, 15°W-60°E, see Fig. 8 of main manuscript). For this larger area the correlations are also high, namely $r = 0.80$ both for September and October. The respective ERs are 0.51 and 0.31, which agrees very well with the values obtained by averaging over individual bins in the region covering southern Africa (see Tab. 4 in the main manuscript).

4 Spatial distribution of correlation coefficients and enhancement ratios for single years

To demonstrate that the spatial features in Figs. 9-13 of the main manuscript, obtained for monthly composites, are generally observable in every single year, we present two single-year results. Figure S11 shows spatial distributions of HCN-CO correlation coefficients (left) and enhancement ratios (right) of February, April, July and October 2008. In each of the four months there are high correlations in the same geographical regions as in Fig. 9 of the main manuscript. Due to the restriction to one

year and application of the same filter criteria as for the monthly composites (consideration of bins with mean CO VMRs $>$ 80 ppbv and with more than 10 points only), the data gaps (white areas) are larger and the areas of high correlation are smaller. However, the enhancement ratios in the areas of high correlation are rather similar to those obtained for the February, April and July composites. In the area of southern hemispheric pollution during October they are somewhat lower than for the October composite, indicating less progressed plume aging.

Figure S12 shows the geographical distribution of C_2H_2-HCN correlation coefficients (left) and enhancement ratios (right) of February, April, August and October 2003. Here, an even better agreement with the monthly composites presented in Fig. 10 of the main manuscript can be seen, both for the correlation coeffcients and the ERs. Somewhat larger differences are, e.g., visible between the ERs above the southern tropical Atlantic during October. In this region the single-month values presented here indicate a less progressed plume aging than those of the October composite shown in the main manuscript.

References

Justice, C.O., Giglio, L., Korontzi, S., Owens, J., Morisette, J.T., Roy, D., Descloitres, J., Alleaume, S., Petitcolin, F. and Kaufman, Y.: The MODIS fire products, Rem. Sens. Env., 83, 244–262, 2002.

Zängl, G. and Hoinka, K. P.: The Tropopause in the Polar Regions, Bull. Amer. Meteor. Soc., 14, 3117–3139, 2001.

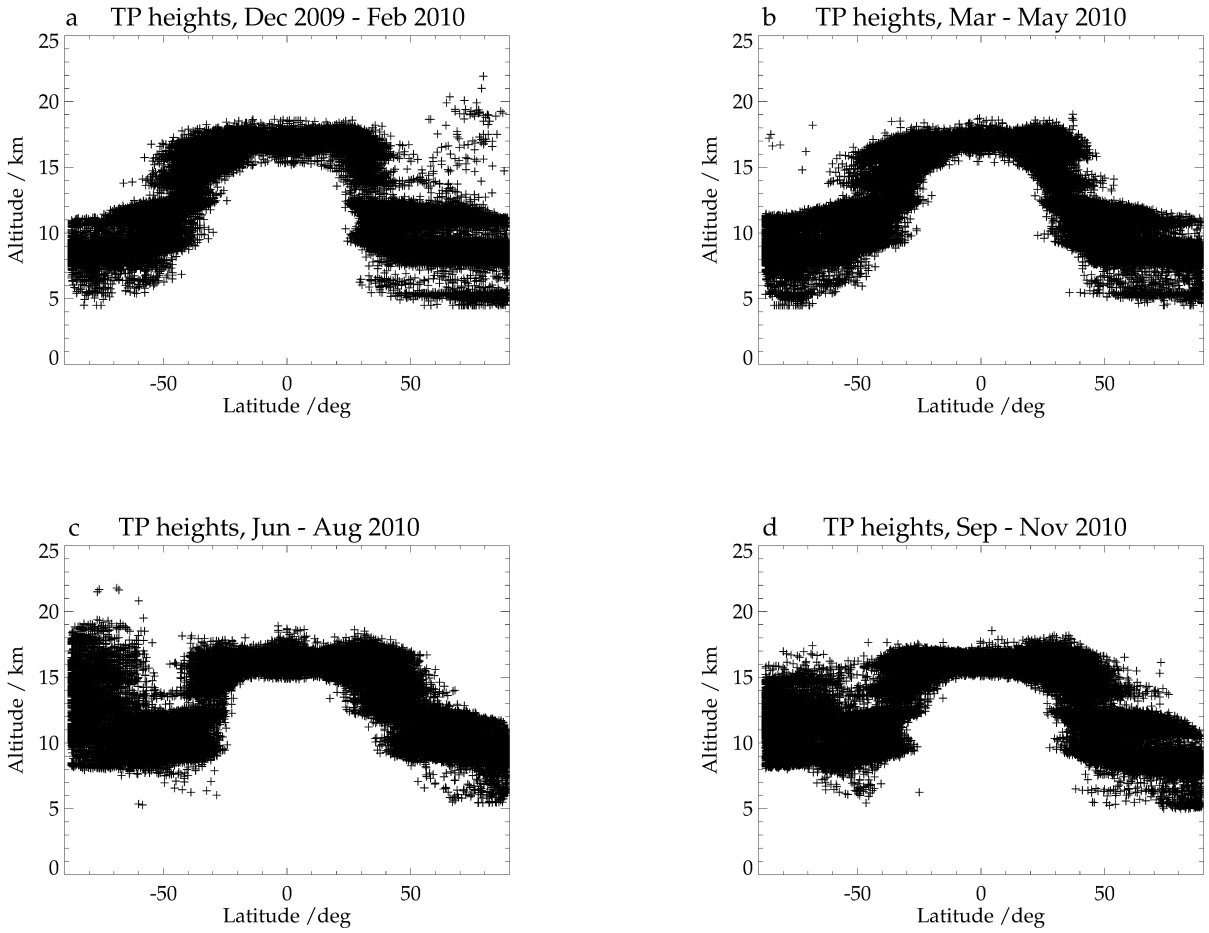

Figure S1. Heights of the thermal tropopause derived from MIPAS temperature profiles for the periods **(a)** December 2009 to February 2010, **(b)** March to May 2010, **(c)** June to August 2010, and **(d)** September to November 2010.

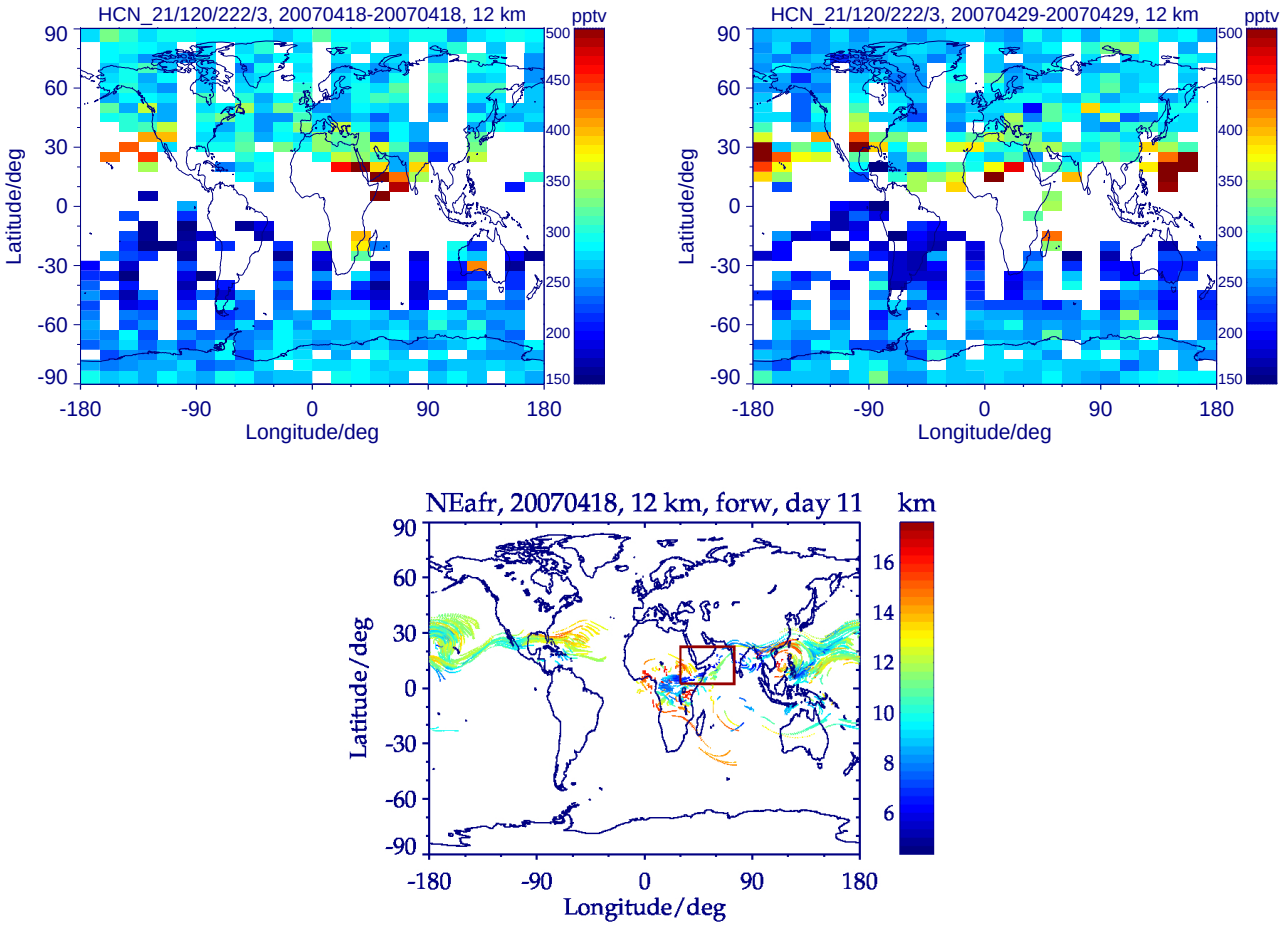

Figure S2. Top row: Global HCN distributions at 12 km altitude, measured by MIPAS on 18 April (left) and on 29 April 2007 (right). Bottom: 12-day HYSPLIT forward trajectories, started on 18 April 2007, 0:00 UT, in the region of the HCN plume above North-East Africa (marked by red margin) at 12 km altitude. The trajecties are colour coded by altitude. Only the end sections of the trajectories covering the 29th of April are shown.

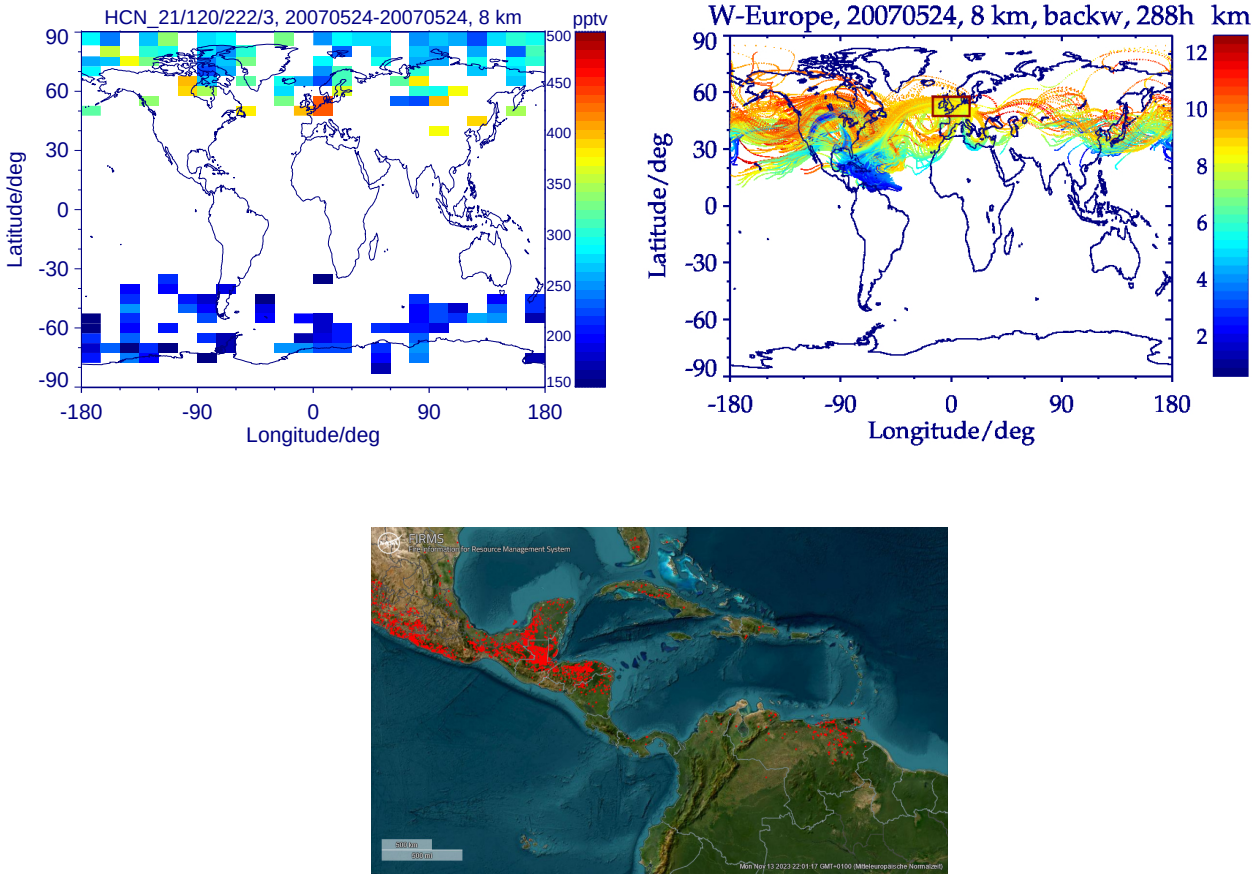

Figure S3. Top left: Global HCN distribution at 8 km altitude, measured by MIPAS on 24 May 2007. A plume of enhanced HCN is visible over Western Europe. Top right: HYSPLIT 12-day backward trajectories, started on 24 May, 12:00 UT, in the plume region (marked by red margin) at 8 km altitude. The trajecties are colour coded by altitude. Bottom: FIRMS fire counts from 12–13 May, 2007, in Central America.

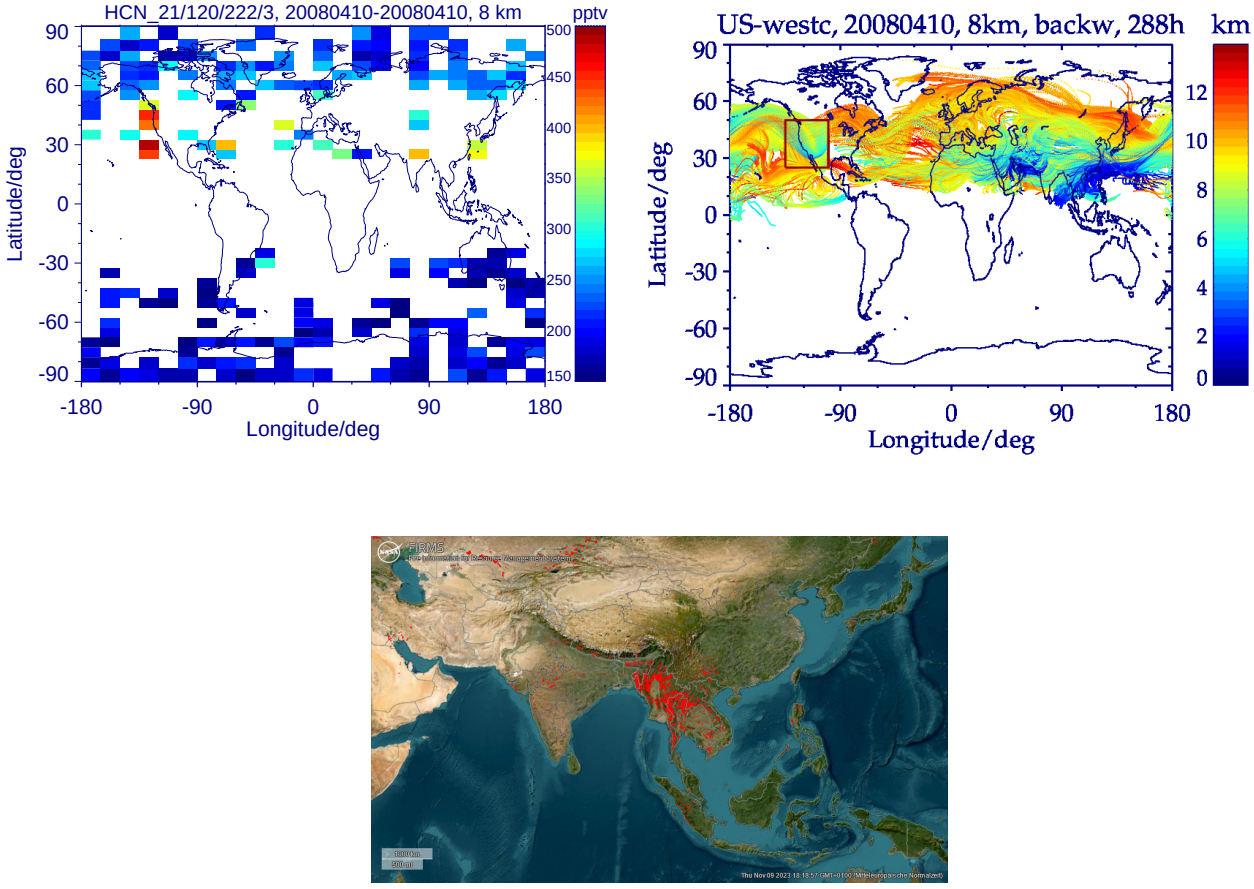

Figure S4. Top left: Global HCN distribution at 8 km altitude, measured on 10 April 2008. A plume of enhanced HCN is visible at the West Coast of the United States. Top right: HYSPLIT 12-day backward trajectories started on 10 April 2008, 12:00 UT, in the plume region (marked by red margin) at 8 km altitude. The trajecties are colour coded by altitude. Bottom: FIRMS fire counts from 29 March 2008 in South-East Asia.

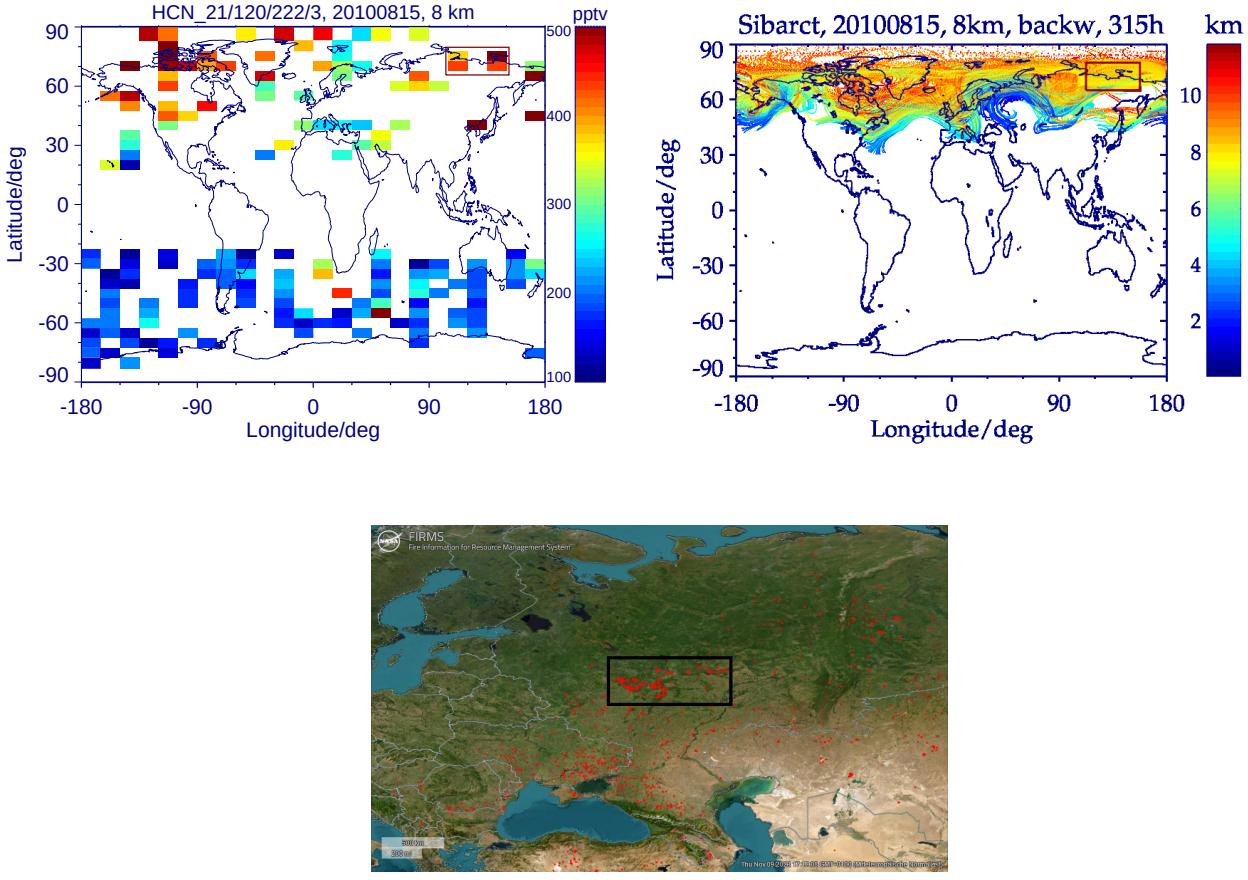

Figure S5. Top left: MIPAS HCN distribution at 8 km altitude, measured on August 15, 2010. Top right: HYSPLIT 13-day backward trajectories started on August 15, 2010, 0:00 UT, in the region of the HCN plume in North-East Siberia (marked by red margin), colour-coded by altitude. Bottom: FIRMS fire counts from August 3, 2010, in Eastern Russia. A region of intense peat fires south-east of Moscow is marked by a black rectangle.

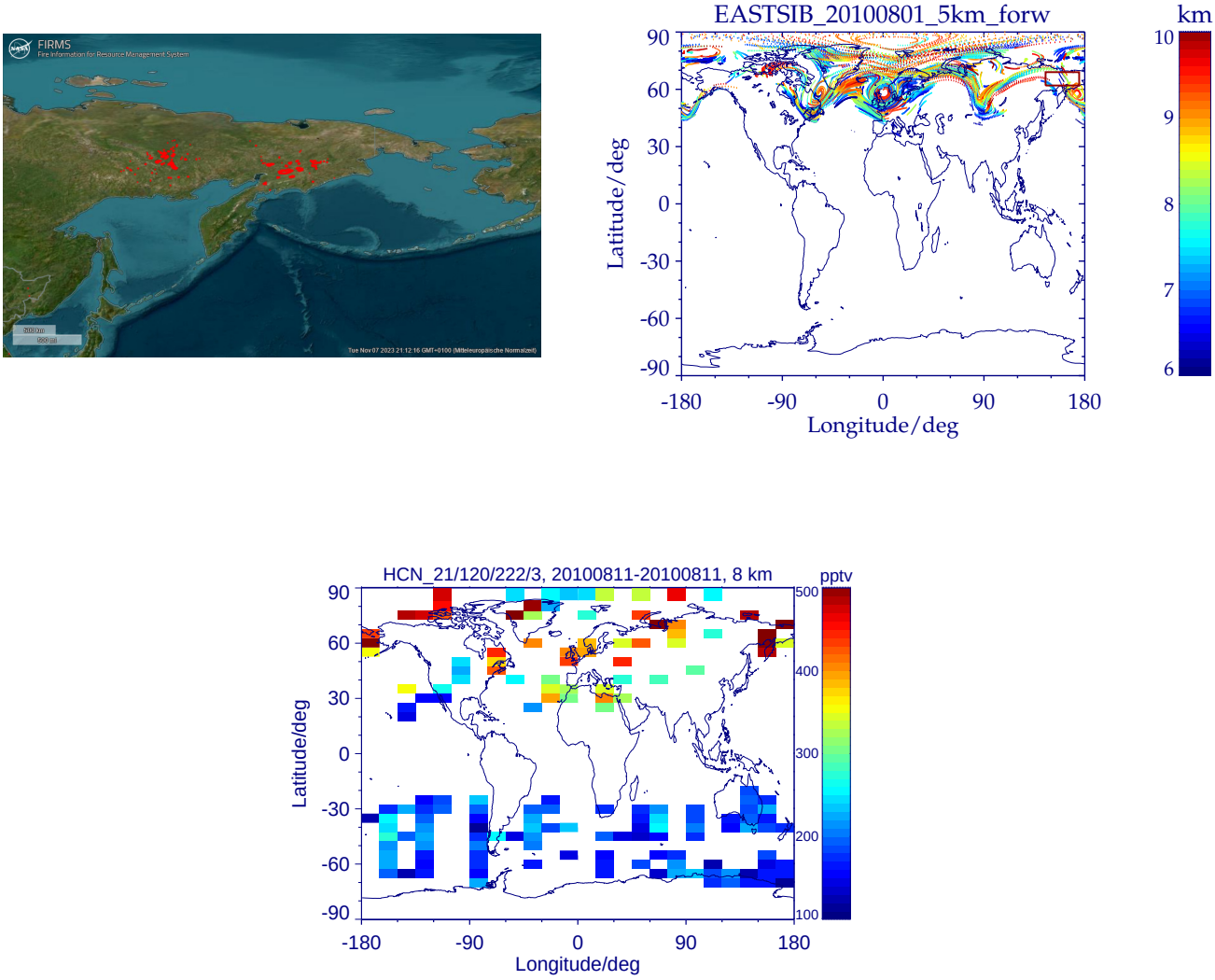

Figure S6. Top left: FIRMS fire counts from 1 August 2010 in North-East Siberia. Top right: HYSPLIT 11-day forward trajectories started on August 1, 2010, 0:00 UT, at 5 km altitude above the fire region (marked by red margin), colour-coded by altitude. Only the sections of the trajectories covering the 11th of August are shown. Bottom: MIPAS HCN distribution at 8 km altitude, measured on August 11, 2010.

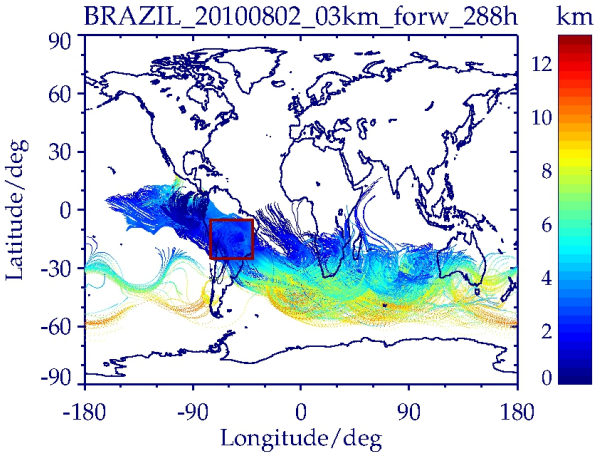

Figure S7. HYSPLIT 12-day forward trajectories started on August 2, 2010, at 3 km altitude above tropical South America.

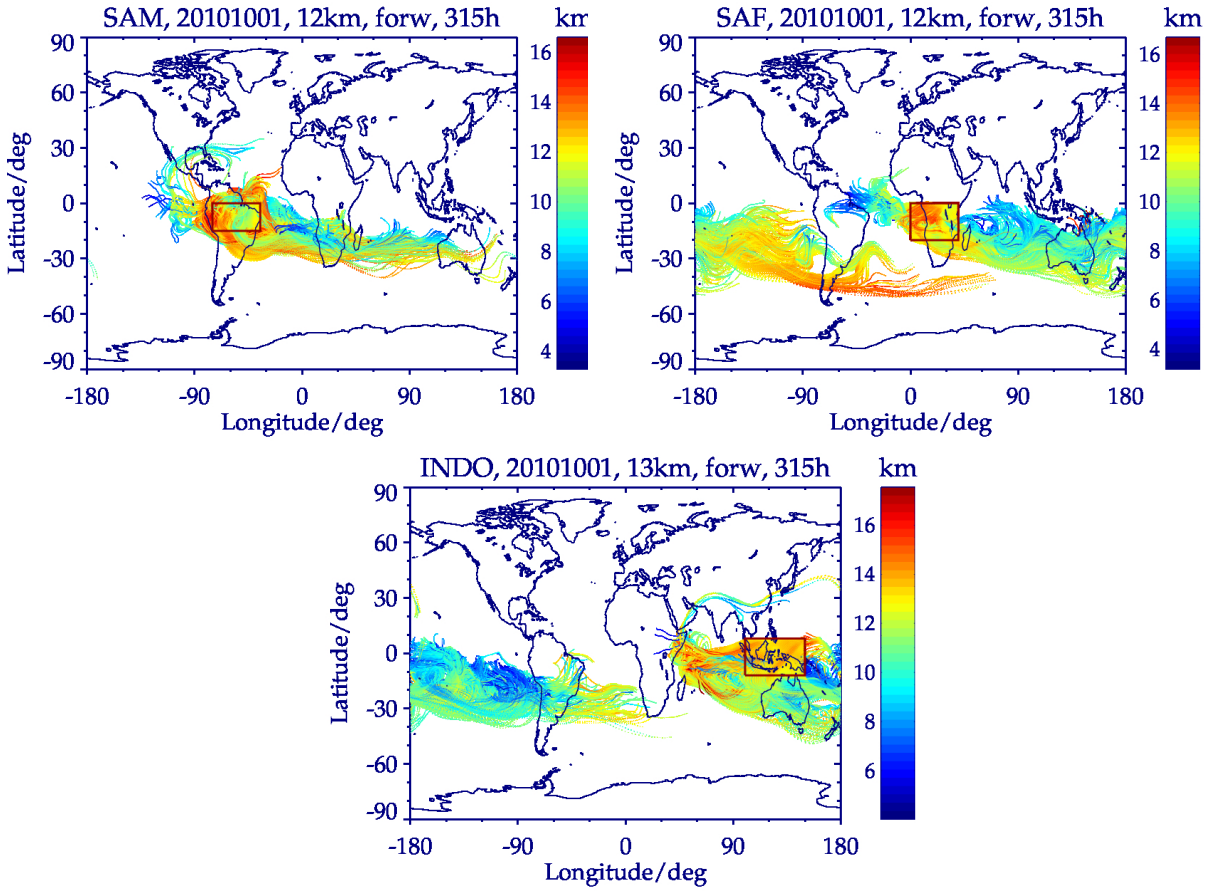

Figure S8. HYSPLIT 13-day forward trajectories started on October 1, 2010, at 12 km altitude above the South American (top left) and the South African (top right) biomass burning region. Bottom: 13-day forward trajectories started on October 1, 2006, at 13 km altitude above the Indonesian biomass burning region.

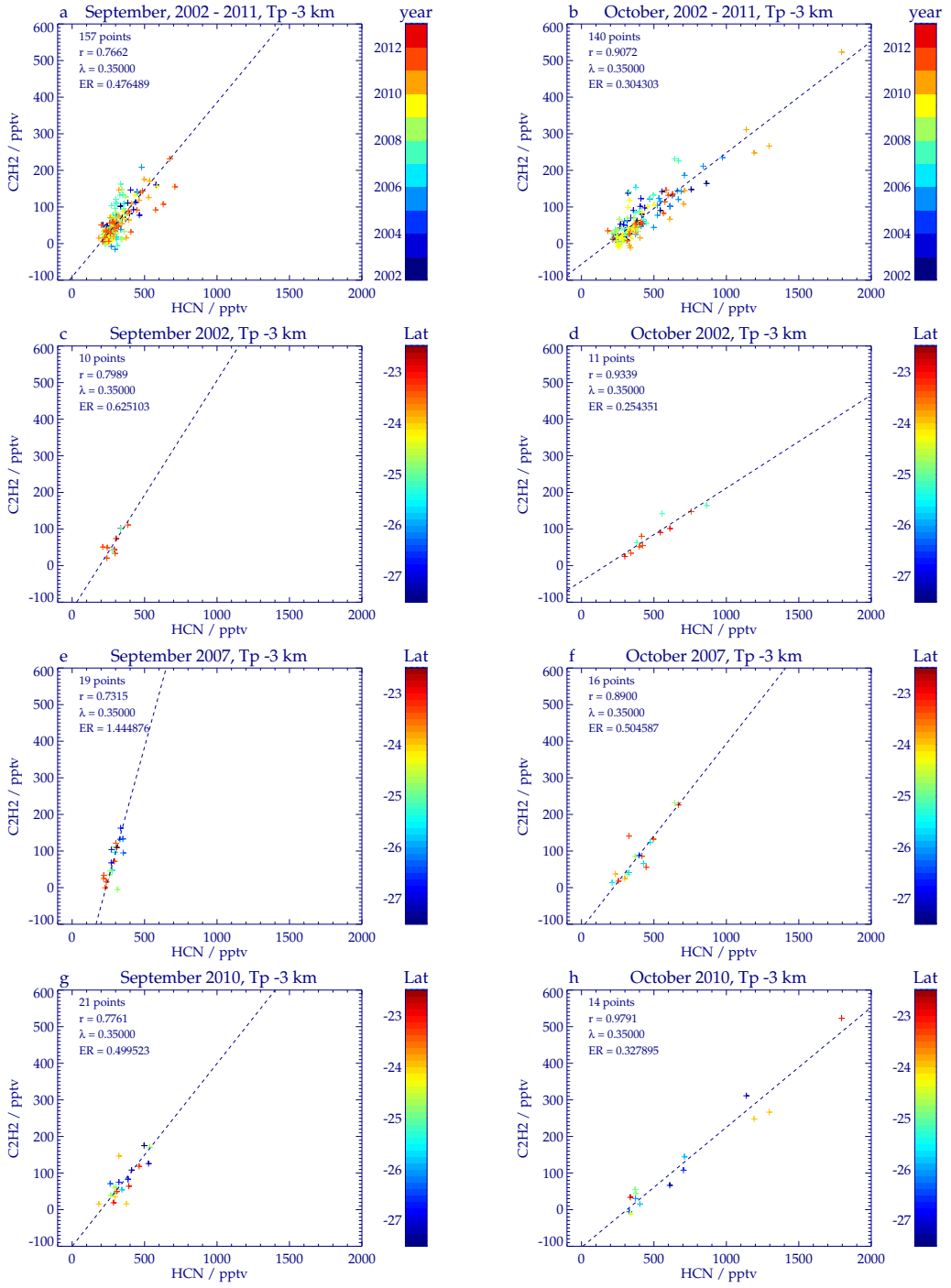

Figure S9. Top row: Correlation plots between **(a)** September and **(b)** October composites (right) of MIPAS C_2H_2 and HCN at 3 km below the tropopause for measurements in a bin between Mozambique and southern Madagascar (27.5°S-22.5°S, 30°E-45°E, see Fig. 10 of the main manuscript). Given in the legend are the number of data pairs, the Pearson correlation coefficient *r*, the applied λ value and the fitted enhancement ratio ER. Second, third and bottom row: Same as upper row, but for September/October **(c, d)** 2002, **(e, f)** 2007 and **(g, h)** 2010.

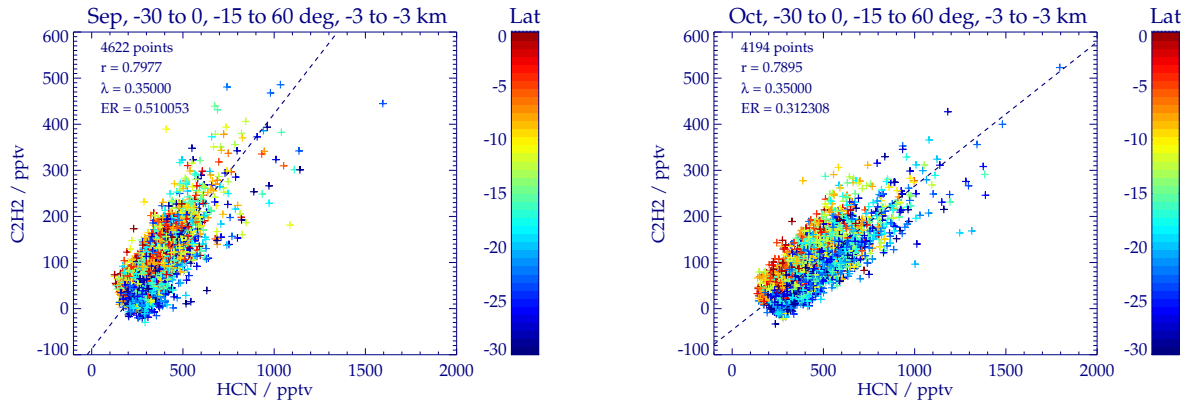

Figure S10. Correlation plots between September (left) and October composites (right) of MIPAS C_2H_2 and HCN at 3 km below the tropopause for southern Africa (30°S-0°S, 15°W-60°E). For further details see Fig. S9.

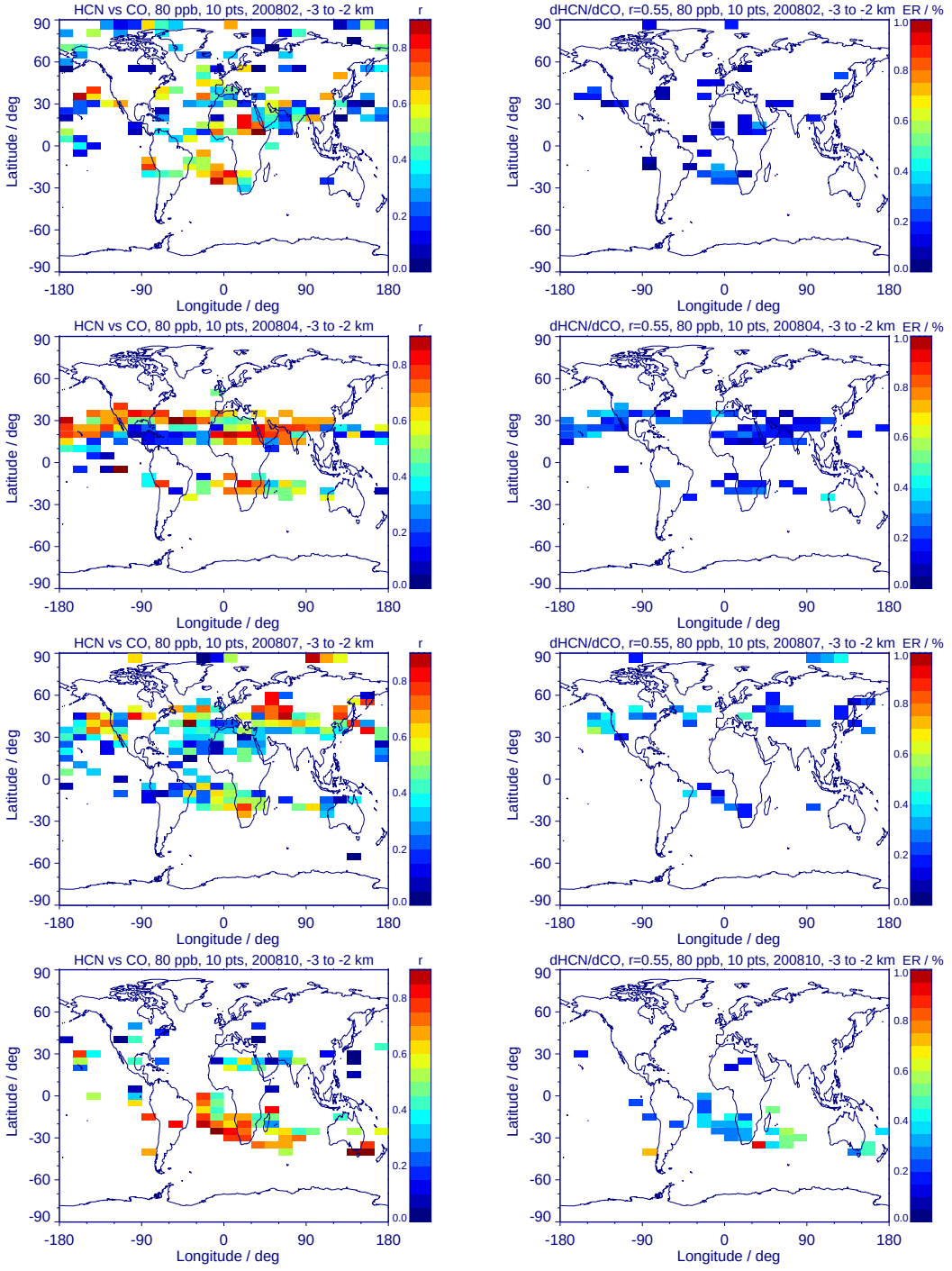

Figure S11. Left: Global distribution of correlation coefficients *r* between MIPAS measurements of HCN and CO in the upper troposphere, for **(a)** February, **(c)** April, **(e)** July and **(g)** October 2008. Right: Corresponding ΔHCN/ΔCO enhancement ratios (ER) in 0.01 pptv/pptv for **(b)** February, **(d)** April, **(f)** July and **(h)** October 2008. White areas are bins with mean CO VMRs lower than 80 ppbv (no significant CO enhancement), with less than ten data points or with negative correlation coefficients. The bin-size is 5° latitude × 15° longitude. The displayed altitude is 3 km (50°S to 50°N) and 2 km (higher latitudes) below the tropopause.

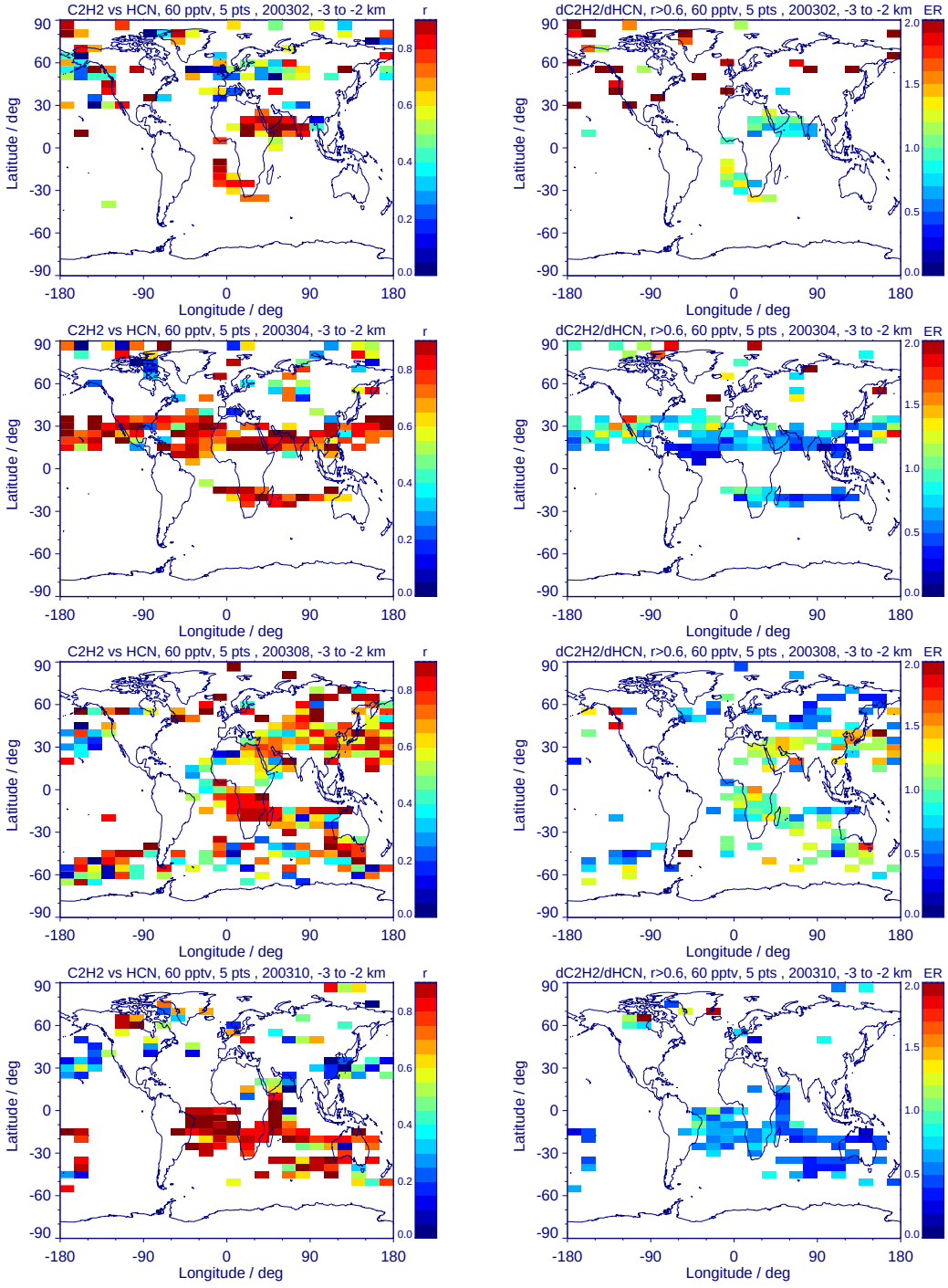

Figure S12. Left: Global distribution of correlation coefficients *r* between MIPAS measurements of C_2H_2 and HCN in the upper troposphere, for **(a)** February, **(c)** April, **(e)** August and **(g)** October 2003. Right: Corresponding $\Delta C_2H_2/\Delta HCN$ enhancement ratios (ER) in pptv/pptv for **(b)** February, **(d)** April, **(f)**August and **(h)** October 2003. White areas are bins with mean C_2H_2 VMRs lower than 60 pptv (no significant C_2H_2 enhancement), with less than five data points or with negative correlation coefficients. For further details see Fig.S11.